Optimization of carbon nanotube ultracapacitor for cell design

Antonis Orphanou, Toshishige Yamada, and Cary Y. Yang

Citation: Journal of Applied Physics **119**, 214311 (2016); doi: 10.1063/1.4953224
View online: http://dx.doi.org/10.1063/1.4953224
View Table of Contents: http://scitation.aip.org/content/aip/journal/jap/119/21?ver=pdfcov
Published by the AIP Publishing

Optimization of carbon nanotube ultracapacitor for cell design

Antonis Orphanou,[1,a)] Toshishige Yamada,[2,a)] and Cary Y. Yang[1]
[1]*Center for Nanostructures, Santa Clara University, Santa Clara, California 95053, USA*
[2]*Electrical Engineering, Baskin School of Engineering, University of California Santa Cruz, Santa Cruz, California 95064, USA*

(Received 29 March 2016; accepted 23 May 2016; published online 7 June 2016)

We report a methodology to optimize vertically grown carbon nanotube (CNT) ultracapacitor (CNU) geometrical features such as CNT length, electrode-to-electrode separation, and CNT packing density. The electric field and electrolyte ionic motion within the CNU are critical in determining the device performance. Using a particle-based model (PBM) based on the molecular dynamics techniques we developed and reported previously, we compute the electric field in the device, keep track of the electrolyte ionic motion in the device volume, and evaluate the CNU electrical performance as a function of the aforementioned geometrical features. We show that the PBM predicts an optimal CNT density. Electrolyte ionic trapping occurs in the high CNT density regime, which limits the electrolyte ions from forming a double layer capacitance. In this regime, the CNU capacitance does not increase with the CNT packing density as expected, but dramatically decreases. Our results compare well with existing experimental data and the PBM methodology can be applied to an ultracapacitor built from any metallic electrode materials, as well as the vertical CNTs studied here. *Published by AIP Publishing*. [http://dx.doi.org/10.1063/1.4953224]

INTRODUCTION

The study of ultracapacitors (UC) or supercapacitors has been the subject of intense research in recent years.[1–3] Increasing the total capacitor electrode surface area S to maximize the device stored energy has always been a prohibitive challenge. The use of nanomaterials as capacitor electrodes has been studied recently,[4–14] as many of these materials are low-dimensional and, when properly integrated onto a metallic electrode substrate, S increases significantly. Such low-dimensional nanomaterials can be metallic or semiconducting, just like their macroscopic counterparts, with some notable exceptions. For example, silicon chains are not semiconducting but generally metallic. Thus, careful examination of the suitability of materials to serve as capacitor electrodes is required.[15–17] Graphite (3-D) is metallic, and so is graphene (2-D), but carbon nanotubes (CNTs) (1-D) can be either metallic or semiconducting.[18] When semiconducting nanotubes are contacted to metal electrodes, Schottky or tunneling barriers can be created[19–22] and achieving low-resistance ohmic contact is a major challenge. Nevertheless, there are many studies on UCs using nanocarbons,[4,5,22] as their chemically inert surfaces do not require electrode passivation layers. Initially, UCs were made of porous carbons.[6] Subsequently, activated carbons,[7] nanotubular materials,[8] CNTs,[9] carbon aerogel composites,[10] fibrous carbon,[11] carbon/graphene nanotube composites,[12] and graphene[13] were investigated as alternative electrode materials. Most UCs contain an electrolyte since capacitance significantly increases with its inclusion, due to the formation of a double layer capacitance (DLC), which is the capacitance between the electrolyte ions and the electrode charges separated by nanoscale distances.[14,23–27] The DLC formation can also be interpreted as an effect of screening by electrolyte ions from electrode charges, since, if such charges are perfectly screened, the electric field in the capacitor volume is zero.

Capacitor performance is often evaluated with a Ragone plot of energy density versus power density.[28] Conventional capacitors generally possess power densities higher than 10^4 W/kg, but a low energy density typically in the 0.01–0.05 W h/kg range, making it unsuitable for high-performance energy storage applications.[29] It was recently reported[13] that by using graphene to increase S, UCs can yield as much as 86 W h/kg, thus demonstrating significant potential for nanocarbon UCs. Vertically aligned or randomly oriented CNT arrays or graphene sheets have been shown to increase S and the capacitor energy storage capacity drastically.[30–32]

We study the performance of UCs with electrodes comprised of conducting nanomaterial with a high aspect ratio protruding from and densely packed on conducting surfaces. CNTs possess such properties and thus are among the most suitable electrode materials. The electrode corrugations are so abrupt and dense that the electric field and electrolyte ion spatial distribution within the device cannot be assumed uniform or symmetric in response to an electrical signal. In other words, the DLC would not be formed uniformly along the electrodes due to the abrupt and dense electrode CNT corrugations. This is in sharp contrast to traditional commercial UCs, in which the corrugations are smooth, shorter in length, and not as dense. One of the well accepted models, proposed by de Levie,[33] is an analytical equivalent-circuit-based compact model, most suited for the analysis of these commercial UCs with smooth corrugations. Under the de Levie model assumptions, due to the "smooth" nature of the electrode, the DLC is uniformly and symmetrically formed

[a)]Authors to whom correspondence should be addressed. Electronic addresses: aorphanou@scu.edu and tyamada@soe.ucsc.edu

following the contour of the electrode surfaces. Under these conditions, it is reasonable to assume the electrolyte as a homogeneous neutral jellium, suitable for invoking the de Levie model. However, in many nanomaterial-based UCs, changes in corrugations are abrupt and significant. Therefore, we can no longer assume that the electrolyte is spatially uniform or the electric field is uniform along the electrodes or within the capacitor. Thus, the formation of the DLC will have to be re-examined using a new approach that can potentially resolve the existing model limitations, as described above. This is critical in understanding UC response to an AC voltage input, which is known as the device Nyquist characteristics.[1] We examine these electrode non-uniformities in detail using examples of carbon nanotube ultracapacitors (CNUs) where long and dense CNT arrays protrude from conducting surfaces. For such a study, it is not appropriate to use the homogeneous neutral jellium model for the electrolyte which predicts a smooth DLC formation. Long protrusions are electrically "singular," which violate the assumption of a spatially uniform electrolyte.

Currently, UC modeling is still in its primitive stage. There is no systematic way to identify device resistance, capacitance, and inductance values of a CNU from the electrolyte ionic information or the device geometrical features. Many existing UC modeling studies[34–36] simply aim to recover the measured impedance as a function of frequency, i.e., express Nyquist characteristics using an empirical equivalent circuit for traditional UCs with smooth corrugations. The impedance of the CNU with long CNT cylinders protruding on electrode surfaces cannot be systematically determined using equivalent circuit models. Changes in the UC structure or the electrolyte mass and/or volume density is equivalent to those in the resistance, inductance, and capacitance of the UC model, and empirical equivalent circuit models cannot meet this objective. Thus, the existing UC models are not adequate for our study. To mitigate the scarcity of such approach, we have recently developed a particle-based physical model, using molecular dynamics (MD),[1,37,38] which yielded results that compared well with the existing experimental data.[39] Such a model enables us to calculate the electric field between the electrodes, keep track of the electrolyte ionic motion in the capacitor, and evaluate the device parameters and performance under an arbitrary set of geometrical parameters, electrolyte properties, and voltage excitation.

In this article, following the development of our MD algorithm in Ref. 1, we apply this model to investigate the relationship between CNU capacitance and electrode geometry. In particular, we examine the dependence of CNU linear capacitance density CD_L (in farad per unit electrode width) on electrode-to-electrode separation L_y, CNT length L_{CNT}, and CNT linear packing density D_{CNT} (ratio of CNT diameter d to CNU cell width W_C), and compare our simulated results with available experimental data.[40] Our results show that there is an optimal D_{CNT} range above which CD_L drops dramatically, even below that of the equivalent parallel-plate capacitor (when $L_{CNT}=0$). This behavior is attributed to the formation of an electrolyte ionic trap near the CNT base, which occurs at a CNT-to-CNT separation of approximately $(2/3)L_{CNT}$. The proximity of CNTs at this separation creates too large a potential barrier between adjacent CNTs for the electrolyte ions to overcome, which are in turn trapped and prevented from participating in the formation of a DLC. This and other findings reported here serve to enhance our understanding of the CNU performance that can lead to development of necessary guidelines for eventual CNU cell design.

MODELING AND SIMULATION METHODOLOGY

Using the method reported previously,[1] we solve for the electric field between the nanostructured metallic electrodes. The method is essentially a Poisson equation solver using the MD based techniques with a boundary condition defined at the electrode surface, whose potential takes designated values consistent with the CNU device voltage input. We use MD to subject the device electrode charges (as a coupled system of two electrodes) to the Coulomb forces dictated by the device applied voltage and then allow them to relax to their equilibrium locations.[38,39] This is how electric field in the UCs volume is obtained. In the present PBM, we then keep track of electrolyte ionic motion as dictated by the aforementioned device electric field, and convert it to device output current. By defining the input voltage and computing the output current, it is straightforward to evaluate the device performance. It is obvious in this methodology that the electrode material can be anything as long as it is conducting. We will study CNTs for demonstration purposes, but the nanostructured electrode can be anything made of a conducting material. There are recent reports of UCs using new nanostructured electrode materials,[41,42] and the methodology described here can apply to those and other UCs with different electrode materials.

Our previous calculations confirmed that the electrolyte ionic motion was described successfully and yielded CNU impedance that compared well with experiment.[1,39] Using a similar approach here, we have developed a methodology that can quantify the CNU performance as a function of each of the geometrical variables, L_y, L_{CNT}, and D_{CNT}, as well as cyclic voltammetry (CV) scan rate R_{CV}.[1,39] In determining the CD_L dependence on each of the geometrical parameters, R_{CV} is kept constant.

The performance parameter in this study is the CNU CD_L. Since our model is two-dimensional, CD_L is expressed as capacitance per unit cell width, as opposed to the three-dimensional case where the capacitance density would be defined as the capacitance per unit area. Due to the symmetry of the CNU cell and the cylindrical geometry of CNT, the choice of the transverse or horizontal component of the electric field normal to the CNT sidewall is arbitrary; hence, the 2-D model is an accurate description of the CNU volume.

To closely examine the CNU behavior at high D_{CNT}, we determine the electrolyte ion spatial polarization in the CNU cell in the presence of a sinusoidal applied voltage and the electrolyte ionic distribution and electric field under CV test conditions. These tests are performed with the sole purpose of using the electrolyte ionic motion and distribution to elucidate the contribution of the electrolyte ions in the DLC formation on the electrode surfaces. Further, we compare the

simulated results with experiment for two different CNUs, one having a D_{CNT} twice that of the other.[39] The electrolyte used in all simulations is equivalent to that of a 6 mol/l K^+OH^- solution.

RESULTS AND DISCUSSION

Defining a set of CNU design rules based on the optimization of its performance is critically needed for eventual cell implementation. The analysis presented below elucidates how the CNU geometrical parameters affect the CNU performance and can lead to the optimization of the CNU cell using a set of well-defined design rules. In particular, we report the results of CNU capacitance versus cell parameters, L_y, L_{CNT}, and D_{CNT}, and demonstrate how the simulated electrolyte ionic motion supports and elucidates the predicted CNU performance, using the methodology outlined above and particle model reported in Ref. 1.

CNU performance versus electrode-electrode separation and CNT length

The behavior of CD_L versus L_y is shown in Fig. 1(a) for a unit cell with $W_C = 0.9\ \mu$m, $d = 0.3\ \mu$m, and $L_{CNT} = 1\ \mu$m. CD_L values normalized to its maximum in the simulated unit cell[1] are used throughout. For this unit cell, this maximum occurs at $L_y = 2.2\ \mu$m (minimum L_y) with a value of 7.41 F/m. As expected, this behavior is similar to that of a parallel-plate capacitor, which is inversely proportional to L_y in the case $L_{CNT} = 0$. Fig. 1(b) shows the normalized CD_L versus L_{CNT} for two cell geometries A and B, with $W_C = 0.9\ \mu$m, $d = 0.3\ \mu$m, and $L_y = 3.2\ \mu$m (A) and 6.2 μm (B). The maximum CD_L value of 5.12 F/m at $L_y = 3.2\ \mu$m and $L_{CNT} = 1.455\ \mu$m is used for the normalized CD_L for both A and B. We note that CD_L increases monotonically with L_{CNT} in either case, as longer CNT corresponds to larger S, which is consistent with experimental findings.[43] However, as L_{CNT} increases further and the CNT tips are closer to each other, the increase in CD_L slows, implying that the proximity of the electrodes does not yield any additional improvement in CNU performance. This behavior is attributed to the strong electric field between the CNT tips, which creates a large potential barrier for the electrolyte ions to overcome in traversing the region between the CNT tips. Thus, to avoid this region, the ions move along a path between the electrodes away from the CNT tips, where the potential barrier is lower, resulting in an effective decrease in S that offsets the increase due to a longer CNT. When this occurs, CD_L begins to saturate with further increase in L_{CNT}. As in Fig. 1(a), where CD_L varies approximately with $1/L_y$ for a fixed L_{CNT}, the ratio of saturated CD_L values for A and B matches the reciprocal ratio of their respective L_y values, thus confirming the consistency in our simulated results.

CNU performance versus CV scan rate, simulated results compared with experiment

To demonstrate the utility of our method, we proceed with a comparison of our simulated results with existing experimental data.[40] In particular, simulated and measured CNU capacitances as a function of R_{CV} are compared for two capacitors, X and Y (simulated), and X′ and Y′ (measured), as shown in Figs. 2(a) and 2(b), respectively, where D_{CNT} for X is 0.1, twice that of Y, while X′ has twice the specific surface area as Y′.[40] The vertical axis in Fig. 2(a) is normalized to the maximum simulated CD_L evaluated at $W_C = 3\ \mu$m and $R_{CV} = 40$ mV/s, or 35.08 F/m. The CV ramp rate peak voltage (V_0) is 1.2 V. The normalized measured capacitance density CD (in F/g) for X′ and Y′ versus scan rate are shown in Fig. 2(b).[40] Capacitor X′ contains CNTs with diameters ~5 nm and length 10–20 nm, resulting in a specific surface area of 400 m^2/g. Capacitor Y′ has CNTs 10–20 nm in diameter and 10–50 nm long, for a specific surface area of 200 m^2/g.[40] We assume that the measured capacitance density and the measured specific surface area are proportional to the linear capacitance density and linear packing density, respectively, used in our simulations. The vertical axis in Fig. 2(b) is normalized to the maximum CD value of 110 F/g at a scan rate of ~10 mV/s.[40] Both simulated and experimental cells show that the capacitance density nearly doubles as the CNT density doubles, at least for low scan rates. This

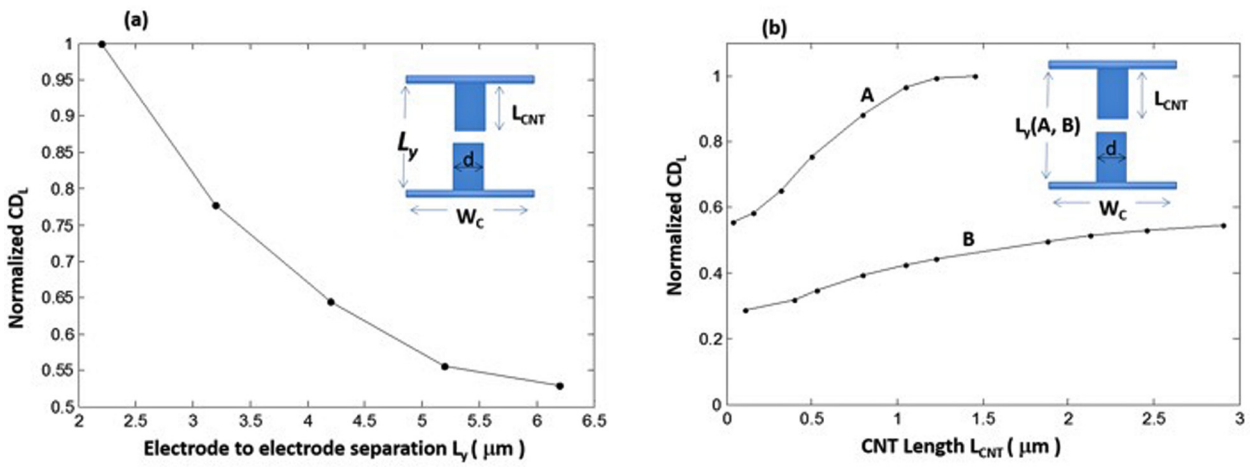

FIG. 1. (a) Normalized simulated CD_L as a function of L_y for a CNU unit cell with $W_C = 0.9\ \mu$m, $d = 0.3\ \mu$m, and $L_{CNT} = 1\ \mu$m. (b) Normalized simulated CD_L as a function of L_{CNT} for a CNU unit cell with $W_C = 0.9\ \mu$m, $d = 0.3\ \mu$m, and $L_y = 3.2\ \mu$m (A) and 6.2 μm (B), respectively. CNU unit cell is shown in the inset. The simulated CD_L plot is normalized to the maximum simulated value.

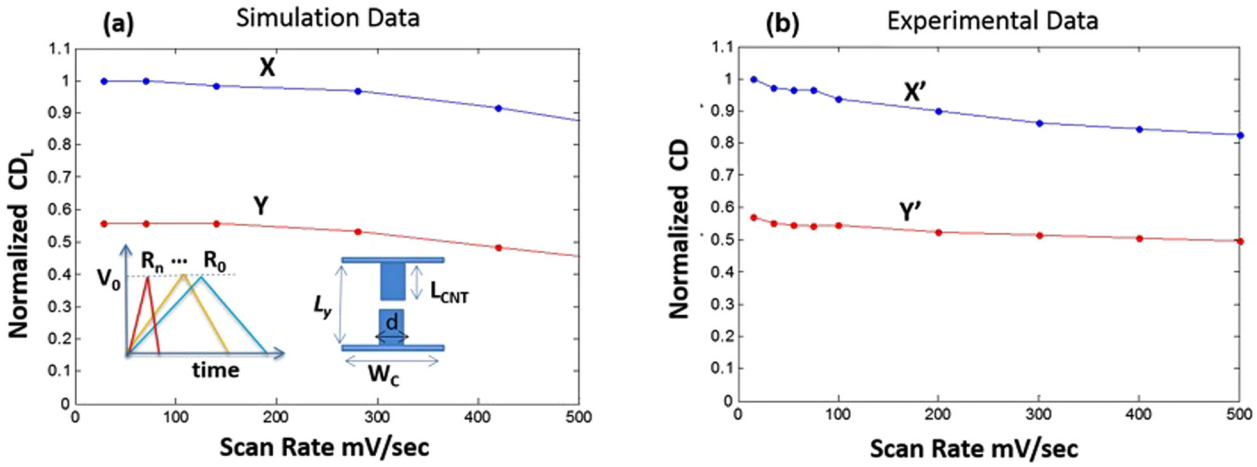

FIG. 2. (a) Normalized simulated CD_L as a function of voltage scan rate for two CNU cells with $D_{CNT}=0.1$ (X) and $D_{CNT}=0.05$ (Y), respectively. The cell dimensions are: $L_y=3.2\,\mu$m, d $=0.3\,\mu$m, $L_{CNT}=1\,\mu$m, $W_C=3\,\mu$m (X) and $6\,\mu$m (Y). (b) Normalized CD for two experimental CNU cells, with X′ having twice the CNT density as Y′.[36] The simulated CD_L plot is normalized to the maximum simulated value.

behavior is expected since the total capacitor area is proportional to the CNT density. However, as the scan rate increases, overcoming the inertia of the electrolyte ions results in slower DLC formation at the electrode surface, leading to decrease in capacitance density, as evidenced in both simulated and measured results.

To provide further comparison with the experiment based on our computed CD_L of 35.08 F/m and using the geometrical scaling rules reported previously,[1] we obtain an estimated CNU energy density of 9 W h/kg, for a 3-D unit cell volume of $W_c \times W_c \times L_y$ and multi-walled CNT on 100 nm Cu film electrodes in an electrolyte solution of 6 mol/l. K^+OH^-. This estimated energy density is within the expected range of an UC[28,44] and comparable to the measured result for a similar CNU.[45] The energy density can be enhanced by optimizing the CNU cell geometry.

CNU performance versus CNT density and analysis of ionic traps

To optimize CNU performance and develop cell design guidelines, one must study the dependence of CD_L on D_{CNT}. In our simulations, we consider three configurations: (1) $L_{CNT}=1\,\mu$m, $d=0.3\,\mu$m, $L_y=3.2\,\mu$m; (2) $L_{CNT}=1\,\mu$m, $d=0.6\,\mu$m, $L_y=3.2\,\mu$m; and (3) $L_{CNT}=1.2\,\mu$m, $d=0.6\,\mu$m, $L_y=3.2\,\mu$m. The results are shown in Fig. 3. The CD_L values are normalized to that for the parallel-plate capacitor ($L_{CNT}=0$), or 2.56 F/m, which is also shown as a reference. The simulations are performed at $R_{CV}=35$ mV/s and $V_0=1.2$ V. Fig. 3 shows that CD_L increases monotonically with increasing D_{CNT}. However, as CD_L continues to increase, we observe a dramatic drop in CD_L. In all three configurations, the sudden decrease in CD_L starts to occur when the CNT-to-CNT separation, $W_s=W_C$-d, is approximately 2/3 the CNT length L_{CNT}. Thus, placing the CNTs at a separation less than (2/3)L_{CNT}, either by increasing d or decreasing W_C as D_{CNT} increases, dramatically reduces the CNU CD_L. This behavior is attributed to electrolyte ionic traps that prevent the ions from participating in the DLC formation near the electrode surface, as a result of the close proximity of the CNTs. Thus, CD_L is significantly reduced at close CNT separations. This decrease in capacitance at high CNT packing density is consistent with reported experimental data for a CNU made of single-walled CNTs.[45,46]

To further examine the ionic trap formation and the decrease in CD_L at high D_{CNT}, we compare the ionic polarizations in the capacitor for two different D_{CNT} values in configuration (1), one having $W_s=0.2\,\mu\text{m}=0.2L_{CNT}$, or high $D_{CNT}=0.6$, and the other $W_s=1.2\,\mu\text{m}=1.2L_{CNT}$, or low $D_{CNT}=0.2$. The two cases are labelled h and l, respectively, in Fig. 4, which illustrates the polarizations for the positive and negative ions in the electrolyte solution, as indicated by the ensemble averages of positive and negative electrolyte ion spatial distributions in the CNU cell. In this simulation, the CNU is subjected to a sinusoidal voltage with amplitude 1.2 V and period 10 s across the electrodes. As shown in Fig. 4, the ionic polarization for high D_{CNT} is much less than that for low D_{CNT}. In the former case, the ionic distributions are confined to the mid-section between the electrodes, which in turn cannot hold a substantial amount of electrolyte charge. Thus, the DLC is diminished significantly. On the other hand, in the low D_{CNT} case, the

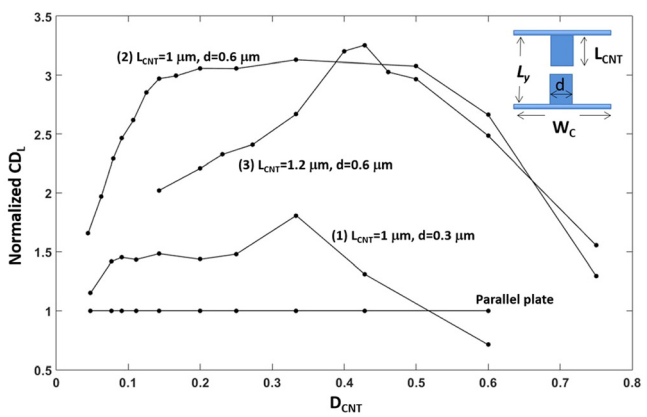

FIG. 3. Normalized simulated CD_L as a function of D_{CNT} for three CNU configurations: (1) $L_{CNT}=1\,\mu$m, $d=0.3\,\mu$m, $L_y=3.2\,\mu$m; (2) $L_{CNT}=1\,\mu$m, $d=0.6\,\mu$m, $L_y=3.2\,\mu$m; and (3) $L_{CNT}=1.2\,\mu$m, $d=0.6\,\mu$m, $L_y=3.2\,\mu$m. CD_L is normalized to the equivalent parallel-plate capacitance density.

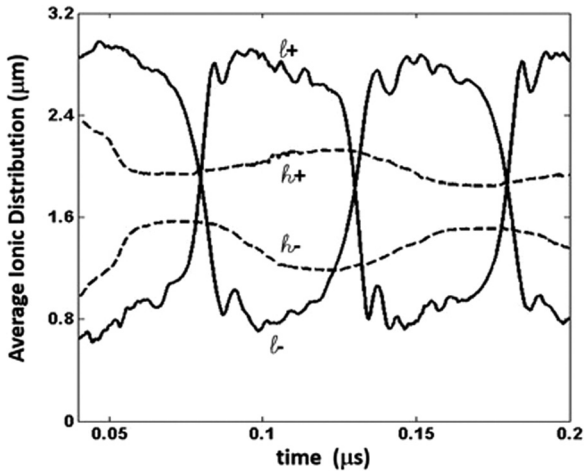

FIG. 4. Ensemble average of electrolyte ionic spatial distributions for the positive (+) and negative (−) ions in the CNU cell, as a function of time for two different D_{CNT} values of configuration (1) defined in Fig. 3. They correspond to: high $D_{CNT} = 0.6$ with $W_s = 0.2\,\mu\text{m} = 0.2L_{CNT}$, indicated by (h+, h−) and low $D_{CNT} = 0.2$ with $W_s = 1.2\,\mu\text{m} = 1.2L_{CNT}$, indicated by (l+, l−).

ensemble averages for both positive and negative ions indicate that they can indeed traverse across the full distance between the electrodes, thus forming a DLC.

The presence of electrolyte ionic traps at high D_{CNT} can be demonstrated with potential contour plots as well as snapshots of electrolyte ionic distribution as illustrated in Figs. 5 and 6, respectively. Fig. 5(a) shows the equipotential contours and the electric field in the capacitor for the low D_{CNT} case. The electric field E is indicated by broken lines orthogonal to the equipotential contours. Fig. 5(b) shows a snapshot of the simulated electrolyte ionic distributions, where the positive ions are indicated in blue and negative ions in red. The potential contours in Fig. 5(a) are consistent with the electrode surface being equipotential. The ionic distributions in Fig. 5(b) display the formation of a DLC near the electrode surface, consistent with the polarization results in Fig. 4.

The equipotential contours and electric field for the high D_{CNT} case are displayed in Fig. 6(a), while Fig. 6(b) shows a similar snapshot of the electrolyte ionic distribution as in the low D_{CNT} case. The results demonstrate that the proximity of adjacent CNTs has significantly impacted the electrical behavior of the CNU. The electric field shown in Fig. 6(a) has a large horizontal or E_x component, consistent with the ionic trap formation between adjacent CNTs, where the magnitude of potential is low. This phenomenon is also consistent with the assertion that the low potential between adjacent CNTs serves to trap the electrolyte ions and restricts their movement, as evident in the snapshot of ionic distributions in Fig. 6(b).

Due to computational limitations, solution of Poisson equation is approximated by a finite number of electrode charges. The more charges used in the electrode molecular dynamics computation, the closer to a continuous electrode

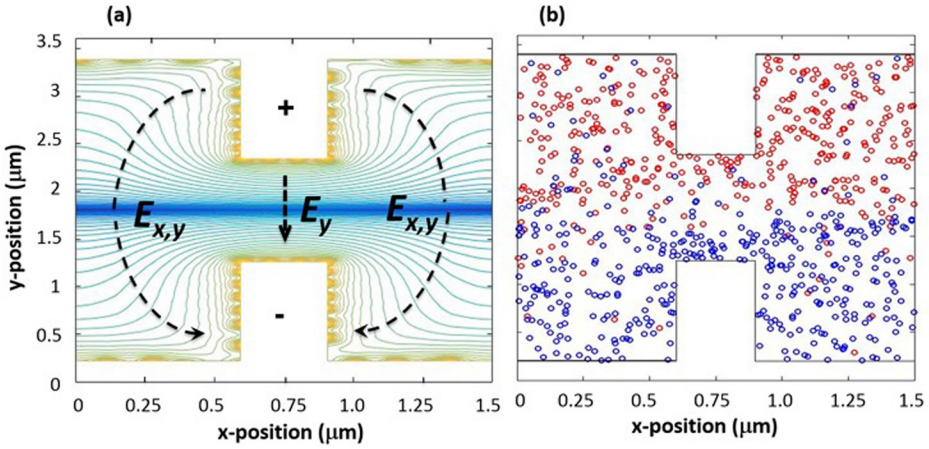

FIG. 5. (a) Computed contours of the electric potential magnitude and the corresponding electric field in the CNU cell for configuration (1), with $W_s = 1.2\,\mu\text{m} = 1.2L_{CNT}$ and $D_{CNT} = 0.2$. (b) Time-evolution snapshot of electrolyte ionic distributions inside the same cell, where positive ions are indicated in blue and negative ions in red.

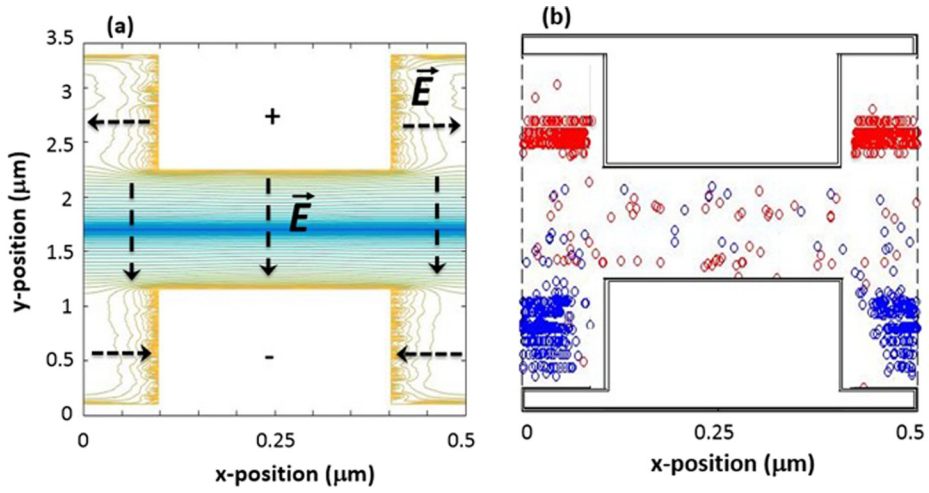

FIG. 6. (a) Computed contours of the electric potential magnitude and the corresponding electric field in the CNU cell for configuration (1), with $W_s = 0.2\,\mu\text{m} = 0.2L_{CNT}$ and $D_{CNT} = 0.6$. (b) Time-evolution snapshot of electrolyte ionic distributions inside the same cell, where positive ions are indicated in blue and negative ions in red.

charge distribution is achieved. As a result, very close to the electrodes, the computed electric field might not display the expected behavior of being normal to the electrode surface, as shown in Figs. 5(a) and 6(a). However, it is demonstrated in similar computations[1,37,38] that such approximation does not affect the principal findings, since in part, in our computational model the electric field is properly restored quickly close to the electrode surface.

Our results can generally apply to any UCs with nanostructured electrodes. This is due to the structure of the computational algorithm and the way it solves for the electric field within the CNU. Different electrode materials simply reduce to a problem solution of the Poisson equation employing the same boundary conditions along the electrode boundary. As long as the electrode is metallic enough, the electric field within the UC volume is independent of the electrode material. While CNU is studied here in depth to demonstrate the utility of our approach, the model and simulation methodology can generally be applied to nanostructure electrodes using other nanocarbon materials such as graphene foam or carbon cloth,[47,48] as well as metal oxides Co_3O_4, MnO_2, Fe_2O_3, ZnO, or carbon decorated ZnO.[41,42]

CONCLUSION

We have investigated the effects of electrode-to-electrode separation, CNT length, and CNT density on the electrical performance of the CNU cell, using a particle-based model. Assuming a metallic and equipotential electrode surface and solving for the electric field in the device using molecular dynamics, we have simulated the electrolyte ionic motion and spatial distributions, computed the capacitor current, and hence determined all electrical parameters. Our results compare well with existing experimental data and the estimated energy density based on the computed CNU capacitance density is consistent with the reported measured values. In addition, the computed capacitance has an optimal range of CNT linear packing density D_{CNT} values, beyond which the performance degrades dramatically, even dropping below the equivalent parallel-plate capacitance, at which $L_{CNT} = 0$ in the capacitor cell. In particular, we have shown that the linear capacitance density CD_L increases with increasing D_{CNT} up to the point where the CNT-to-CNT separation W_s reaches $\sim 2L_{CNT}/3$ before dropping sharply. Such dramatic decrease in CD_L is attributed to the occurrence of electrolyte ionic traps between adjacent CNTs at close proximity. This finding is supported by computed potential contours and electric field, as well as ionic distributions at two different values of D_{CNT}. It is also consistent with the reported experimental data. The approach and the results presented here can lead to a versatile UC model development and definition of guidelines for CNU cell design for eventual implementation.

[1]A. Orphanou, T. Yamada, and C. Y. Yang, Nanotechnology **23**, 095401 (2012).
[2]S. Pang, M. Anderson, and T. Chapman, J. Electrochem. Soc. **147**, 444 (2000).
[3]S. Gupta, M. Hughes, A. H. Windle, and J. Robertson, J. Appl. Phys. **95**, 2038 (2004).
[4]G. Zhou, D. Wang, F. Li, L. Zhang, Z. Weng, and H. Cheng, New Carbon Mater. **26**, 180 (2011).
[5]D. Tashima, M. Taniguchi, D. Fulikawa, T. Kijima, and M. Otsubo, Mater. Chem. Phys. **115**, 69 (2009).
[6]H. Wang and H. Dai, Chem. Soc. Rev. **42**, 3088 (2013).
[7]E. Frackowiak and F. Beguin, Carbon **39**, 937 (2001).
[8]R. Koetz and M. Carlen, Electrochem. Acta **45**, 2483 (2010).
[9]A. Balducci, R. Dugas, P. L. Taberna, P. Simon, D. Plée, M. Mastragostino, and S. Passerini, J. Power Sources **165**, 922 (2007).
[10]E. Frackowiak, K. Jurewich, K. Szostak, S. Delpeux, and F. Beguin, Fuel Process. Technol. **77–78**, 213 (2002).
[11]M. Kaempgen, C. K. Chan, J. Ma, Y. Cui, and G. Gruner, Nano Lett. **9**, 1872 (2009).
[12]G. R. Li, Z. P. Feng, Y. N. Ou, D. Wu, R. Fu, and Y. X. Tong, Langmuir **26**, 2209 (2010).
[13]K. Babe and K. Jurewicz, Fuel Process. Technol. **77–78**, 181 (2002).
[14]C. Liu, Z. Yu, D. Neff, A. Zhamu, and B. Jang, Nano Lett. **10**, 4863 (2010).
[15]T. Yamada, Y. Yamamoto, and W. A. Harrison, J. Vac. Sci. Technol. B **14**, 1243 (1996).
[16]T. Yamada, J. Vac. Sci. Technol. B **15**, 1019 (1997).
[17]T. Yamada, C. W. Bauschlicher, and H. Partridge, Phys. Rev. B **59**, 15430 (1999).
[18]M. S. Dresselhaus, G. Dresselhaus, and P. C. Eklund, *Science of Fullerenes and Carbon Nanotubes* (Academic, London, 1996).
[19]T. Yamada, Appl. Phys. Lett. **76**, 628 (2000).
[20]T. Yamada, Appl. Phys. Lett. **78**, 1739 (2001).
[21]T. Yamada, Appl. Phys. Lett. **80**, 4027 (2002).
[22]T. Yamada, T. Saito, M. Suzuki, P. Wilhite, X. Sun, N. Akhavantafti, D. Fabris, and C. Y. Yang, J. Appl. Phys. **107**, 044304 (2010).
[23]Q. Cheng, T. Tang, J. Ma, H. Zhang, N. Shinya, and L. Qin, Phys. Chem. Chem. Phys. **13**, 17615 (2011).
[24]P. Kurzweil and M. Chwistek, J. Power Sources **176**, 2555 (2008).
[25]E. Frackowiak, G. Lota, and J. Pernak, Appl. Phys. Lett. **86**, 164104 (2005).
[26]J. D. Stenger-Smith, C. K. Webber, N. Anderson, A. P. Chafin, K. Zong, and J. R. Reynolds, Electrochem. Soc. **149**, A973 (2002).
[27]H. Yamada and P. R. Bandaru, Appl. Phys. Lett. **104**, 213901 (2014).
[28]H. Abruna, Y. Kiya, and J. C. Henderson, Phys. Today **61**(12), 43 (2008).
[29]R. Kötz and M. Carlen, Electrochim. Acta **45**, 2483 (2000).
[30]H. J. In, S. Kumar, Y. Shao-Horn, and G. Barbastathis, Appl. Phys. Lett. **88**, 083104 (2006).
[31]P. C. Chen, G. Shen, S. Sukcharoenchoke, and C. W. Zhou, Appl. Phys. Lett. **94**, 043113 (2009).
[32]J. Schindall, IEEE Spectrum **44**, 42 (2007).
[33]R. de Levie, "Electrochemical response of porous and rough electrodes," Advances in Electrochemistry and Electrochemical Engineering (1967), Vol. 6, pp. 329–397.
[34]S. Buller, E. Karden, D. Kok, and R. W. De Doncker, Proc. IEEE Ind. App. Soc. Meet. **4**, 2500 (2001).
[35]T. D. Dongale, P. R. Jadhav, G. J. Navathe, J. H. Kim, M. M. Karanjkar, and P. S. Patil, Mater. Sci. Semicond. Process **36**, 43 (2015).
[36]C. Hao, X. Wang, Y. Yin, and Z. You, J. Electron. Mater. **45**, 515 (2016).
[37]T. Yamada and D. K. Ferry, Phys. Rev. B **48**, 8076 (1993).
[38]T. Yamada and D. K. Ferry, Phys. Rev. B **47**, 6416 (1993).
[39]E. Frackowiak, K. Metenier, V. Bertagna, and F. Beguin, Appl. Phys. Let. **77**, 2421 (2000).
[40]J. H. Kim, K. W. Nam, S. B. Ma, and K. B. Kim, Carbon **44**, 1963 (2006).
[41]X. Zhao, B. Chu, B. Ballesteros, W. Wang, C. Johnston, J. Sykes, and P. Grany, Nanotechnology **20**, 065605 (2009).
[42]X. Jian, G. Chen, C. Wang, L. Yin, G. Li, P. Yang, L. Chen, X. Bao, Y. Gao, and Y. Feng, Nanotechnology **26**, 125705 (2015).
[43]R. Signorelli, D. C. Ku, J. G. Kassakian, and J. E. Schindall, Proc. IEEE **97**, 1837 (2009).
[44]C. Meng, C. Liu, L. Chen, C. Hu, and S. Fan, Nano Lett. **10**, 4025 (2010).
[45]K. Hyeok, W. S. Kim, Y. S. Park, J. M. Moon, D. J. Bae, S. C. Lim, Y. S. Lee, and Y. H. Lee, Adv. Funct. Mater. **11**, 387 (2001).
[46]K. Hyeok, K. K. Jeon, J. K. Heo, C. Lim, D. J. Bae, and Y. H. Lee, J. Electrochem. Soc. **149**, A1058 (2002).
[47]R. Song, H. Jin, X. Li, L. Fei, Y. Zhao, H. Huang, H. L. Chan, Y. Wang, and Y. Chai, J. Mater. Chem. A **3**, 14953 (2015).
[48]Y. Xie, Y. Liu, Y. Zhao, Y. H. Tsang, S. P. Lau, H. Huang, and Y. Chai, J. Mater. Chem. A **2**, 9142 (2014).